Investigation on the Effect of Cooling Rate on Hot Tearing Susceptibility of Al2024 Alloy Using Thermal Analysis

S.G. SHABESTARI and M.H. GHONCHEH

Effect of different cooling rates and Al-5Ti-1B grain refiner on hot tearing susceptibility of Al2024 alloy were studied using thermal analysis. Influence of cooling rates on microsegregation, and the amount of gas and shrinkage porosities was investigated. The cooling rates used in the present study range from 0.4 to 17.5 K s^{-1}. To evaluate the hot tearing susceptibility, Clyne and Davies' criterion is used. To calculate solid fraction during solidification, solid fraction *vs* time is plotted based on Newtonian technique *via* thermal analysis. The results show that the hot tearing susceptibility reduces initially by increasing the cooling rate and then increases at higher cooling rates. Hot tearing susceptibility is decreased by grain refinement. Solidification characteristics of Al2024 *e.g.,* microsegregation, gas, and shrinkage porosities are decreased by increasing cooling rate.

DOI: 10.1007/s11663-015-0450-7

I. INTRODUCTION

THE direct-chill casting (DC) is a semi-continuous casting process presented in 1930s and has been the main production process of high strength aluminum ingots including Al2024 alloy.[1] Because of uneven cooling rate in different regions of the ingot, thermal stresses are generated, which may induce cracks. These cracks may propagate, leading to an ingot failure if the thermal stresses increase. During DC casting of aluminum alloys, the primary and secondary cooling causes strong thermal gradients in the ingot which may lead to distortion of the ingot shape and/or to hot tearing and cold cracking.[2] In DC casting, the name "mushy zone" is misleading, as its top part is actually a slurry, because the newly formed grains are still suspended in the liquid. Only after the temperature has dropped below the coherency temperature, a real mush is formed. The deformation behavior of the mush is very critical for the formation of pores or hot tears.[1,3]

Hot tearing is a common and severe defect encountered in alloy castings. This phenomenon represents the formation of an irreversible crack in the still semi-solid casting.[1,4] Industrial and fundamental studies of this phenomenon show that hot tearing occurs in the late stages of solidification when the volume fraction of solid is above 85 to 95 pct and the solid phase is organized in a continuous network of grains.[1] It is also known that a fine grain structure and controlled casting (without large temperature and stress gradients) help avoid hot cracking.[4]

A number of studies have been conducted to investigate the effects of grain refinement or grain morphology and size on hot tearing.[4,5] However, the results are not consistent and the literature is confusing. Easton *et al.*[6] studied the effect of Ti addition on hot tearing in alloy 6061 by measuring load development in the solidifying test bar. They found that load onset was delayed and the load was lowered with additions of grain refiner. They attributed the delay of strength development to the delay of load transfer due to grain refinement. The mush becomes more pliable (more liquid-like) with the addition of grain refinement, and the point at which the mush behaves more like a solid than a liquid is delayed. Therefore, it reduces the severity of hot tearing. It was concluded that grain refinement decreased hot tearing susceptibility by changing the grain morphology from columnar to equiaxed and reducing the grain size. Easton *et al.*[7] proposed that fine dendritic equiaxed grain morphology in Al cast alloys has the greatest resistance to hot tearing. They also indicated that if grain size was further reduced, the permeability of the mush would decrease, which might cause the hot tearing susceptibility to increase.

Because of the complex mechanisms acting during the solidification of metals, the prediction of the hot tearing phenomenon is not an easy task. The complex nature of mushy properties adds additional difficulties when incorporating these in a hot tearing model.[4,8] Several mechanisms of hot tearing have recently been reviewed. Various criteria that might enable the prediction of hot tears have been proposed. These criteria can be classified into those based on non-mechanical aspects such as feeding behavior, those based only on mechanical aspects, and those that combine these features.[9] Three

S.G. SHABESTARI, Professor, Head, and M.H. GHONCHEH, M.Sc Graduate, are with the Center of Excellence for High Strength Alloys Technology (CEHSAT), School of Metallurgy and Materials Engineering, Iran University of Science and Technology (IUST), Narmak, Tehran 16846-13114, Iran. Contact e-mail: shabestari@iust.ac.ir
Manuscript submitted February 12, 2015.
Article published online September 8, 2015.

criteria based only on non-mechanical aspects are proposed by Feurer,[10] Clyne and Davies,[11] and Katgerman[12]:

(1) Feurer's theory of hot tearing focuses on feeding and shrinkage during solidification.[10] This approach considers that hot tearing occurs due to lack of feeding, which is related to the difficulties of the fluid flow through the mushy zone as a permeable medium competing with solidification shrinkage. This criterion calculates the maximum feeding rate in relation to the shrinkage rate in the vulnerable temperature range.[10]
(2) The hot tearing criterion proposed by Clyne and Davies is based on the assumption of Feurer at the last stage of freezing.[13] It is difficult for the liquid to move freely at the last stage of solidification; so liquid mass feeding cannot accommodate the strains developed during this stage. The last stage of freezing is considered as the most susceptible to hot tearing in this criterion. This criterion is based on the simpler approach of time spent in the vulnerable temperature range.[11,13]
(3) In Katgerman model, theoretical considerations of Clyne and Davies and Feurer are combined.[12]

Also, three criteria based only on mechanical aspects are proposed by Novikov,[14] Prokhorov,[15], and other researchers.[16,17] All of these mechanical criteria introduce an experimentally determined fracture strain that is compared with the thermal contraction and plastic strain (Prokhorov), the thermal contraction strain only (Novikov), and the plastic strain only.

The fundamental cause of chemical inhomogeneity is in the relative movement of solute-rich liquid and solute-lean solid during solidification.[18] Well-adopted mechanism of microsegregation is rejection of alloying elements to the adjacent liquid of solid/liquid interface and formation of chemical composition inhomogeneity called coring.[18,19] The fundamental reason for segregation is the partitioning of solute elements between liquid and solid phases during solidification. In the case of hypoeutectic aluminum alloys (*i.e.*, the majority of commercial aluminum alloys), the liquid phase is enriched in and the solid phase is depleted of solute elements such as Cu, Mg, Zn, Fe, and Si. The so-called partition coefficient, k, of these elements is less than unity, meaning that the concentration of the element in the solid phase is less than in the liquid. In the case of elements with $k > 1$, *e.g.,* Ti in Al, the solid phase becomes enriched during solidification.[20]

Microporosity may be found after solidification, especially in alloys which freeze over a temperature range presenting a dendritic structure, and influences directly the mechanical properties of castings.[21] The dendritic structure is characterized by primary and secondary dendrite arm spacing. Microporosity may occur during solidification of castings either due to rejection of gas from the liquid metal or to the inability of liquid metal to feed through inter-dendritic channels in order to compensate for the shrinkage.[22,23] Analysis of microporosity formation is complex because it depends on inter-dendritic fluid flow and it is affected by parameters such as alloy composition, gas content, casting geometry, and thermal properties of mold, which directly influence the solidification process.[24] As the fluid flow in the inter-dendritic channels depends on the primary and secondary dendrite arm spacing, it is important to know the variation of these parameters during the solidification process to analyze microporosity formation.[25]

In this research, the range of cooling rate between 0.4 and 17.5 K s^{-1} is used to simulate the cooling rate condition utilized in direct-chill casting process. Effect of cooling rates and adding 0.06 wt pct titanium in the form of an Al-5Ti-1B master alloy is evaluated on some defects during solidification of Al2024 alloy, *e.g.,* hot tearing, microsegregation, and porosities. To determine hot tearing susceptibility, Clyne and Davies' criterion is used. To investigate the amount of microsegregation and shrinkage and gas porosities, microstructural evaluation is carried out by optical and scanning electron microscopy.

II. EXPERIMENTAL PROCEDURE

A. *Material and Melting*

Commercial 2024 aluminum alloy was used in this research. Its chemical composition is given in Table I. Seven types of molds having different cooling rates were used to investigate the influence of cooling rate on hot tearing susceptibility and microsegregation in Al2024 alloy (wet and dry sand molds, AISI 1045 steel mold at three different thickness of 0.8, 5, and 10 mm, and water circulated mold to achieve higher cooling rates). Cooling rates condition applied in direct-chill casting process was simulated physically using a designed water-circulated steel mold. Dimensions of the mold were 60 mm in diameter and 80 mm in height. It has been illustrated in Figure 1. In each experiment, 500 g of Al2024 alloy was melted in an electric resistance furnace and the melt was maintained at a temperature of 1023 K ± 5 K (750 °C ± 5 °C). Then, oxide layer was skimmed from the surface of the melt and the molten metal was cast into the molds. Samples were solidified in wide range of cooling rates from 0.4 to 17.5 K s^{-1}. In each cooling rate, three samples were cast, in order to check the reproducibility and the accuracy.

Also, another melting operation was performed by adding 0.06 wt pct Ti in the form of an Al-5Ti-1B rod master alloy. Al-5Ti-1B was added to the melt and after 4 minutes, it was degassed with a nitrogen-base tablet for 5 minutes. It was regularly stirred to achieve a homogenized melt. In this condition, degasser tablet was used to minimize the amount of gas porosities. Variation of shrinkage porosities by changing the cooling rate conditions was measured in grain refined samples. In each experiment, three samples were cast.

Table I. Chemical Composition of 2024 Aluminum Alloy

	Elements (Weight Pct)					
Alloy Composition	Cu	Mg	Mn	Fe	Si	Al
Al2024 alloy	4.33	1.45	0.63	0.23	0.16	bal.

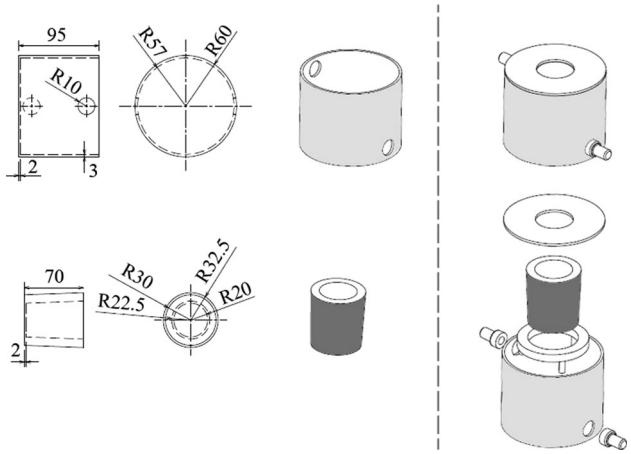

Fig. 1—Dimensions of circulated water mold, (units in mm).

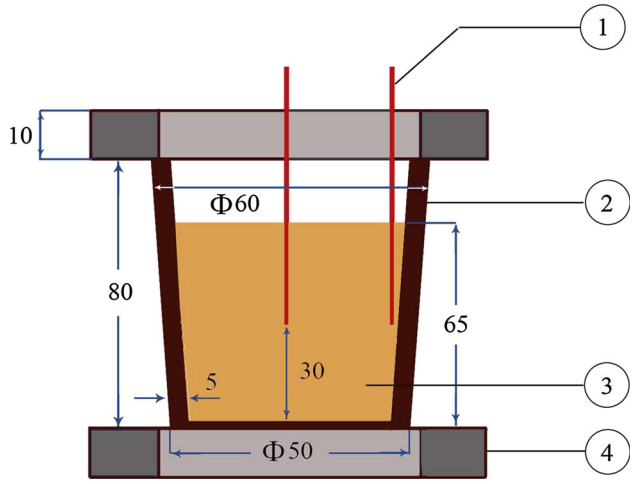

Fig. 2—Experimental setup, (1: thermocouple, 2: crucible, 3: molten metal, and 4: insulation board).

B. *Thermal Analysis and Solid Fraction Curves*

K-type thermocouples (chromel-alumel) manufactured by OMEGA* engineering company were used. They were inserted into a stainless steel sheath and connected to a high-speed data acquisition system. To detect dendrite coherency time, two thermocouples were used; one located at the center of the mold, and the other located near the inner wall. Thermocouples were fixed at exactly the same depth in the melt (at a location of 20 mm from the bottom of the mold). Analog to digital (A/D) convertor used in this work has a sensitive 16-bit convertor (resolution of $1/2^{16}$ or 0.0015 pct), response time of 0.02 seconds, and high accuracy detection. Thermal analysis program can simultaneously display the cooling curves, temperature, and time on the monitor of the computer for an instant observation. Temperature-time data were recorded with the frequency of 10 readings per second. Cooling curve and temperature differences between the wall and the central regions of the mold ($\Delta T = T_w - T_c$) *vs* time curve were plotted using Origin pro.8.6 software**. The adjacent averaging method was applied to each data to smooth the thermal analysis curves. Solid fraction *vs* time was plotted using TAW software which is set based on Newtonian method. Thermocouples were calibrated with melting and solidifying high purity aluminum (99.99 wt pct Al). Figure 2 shows the thermal analysis cup and other components including the lid and attached thermocouples.

*OMEGA Engineering inc, Stamford, Connecticut.

**Origin Lab Corporation, Northampton, MA.

C. *Microstructural Evaluation*

All samples were sectioned horizontally through the place that the tip of the thermocouples was located and prepared for metallographic study. They were mechanically polished, and then etched for metallographic observations. Keller's reagent (5 mL hydrofluoric acid, 10 mL hydrochloric acid, 20 mL nitric acid and 65 mL water) was used for microstructural study. The prepared surfaces were studied using Tescan-Vega II scanning electron microscope (SEM). Furthermore, to measure solidification defects *e.g.,* microsegregation, gas, and shrinkage porosities, Clemex vision PE 3.5 software (Clemex Technologies Inc., Longueil, Quebec, Canada) was used. The Brinell hardness of the specimens was measured under a 31.25 kgf with 2.5 mm diameter of steel ball. The holding time to carry out the hardness test was 30 seconds.

III. RESULTS AND DISCUSSION

A. *Effect of Cooling Rate on Shrinkage and Gas Porosities*

As seen in Figures 3 and 4, area fraction of shrinkage porosities reduces considerably by increasing the cooling rate in grain refined samples. At cooling rate of 17.45 K s^{-1}, the shrinkage porosity in the sample is close to zero (Figure 3(e)). The main reason for the

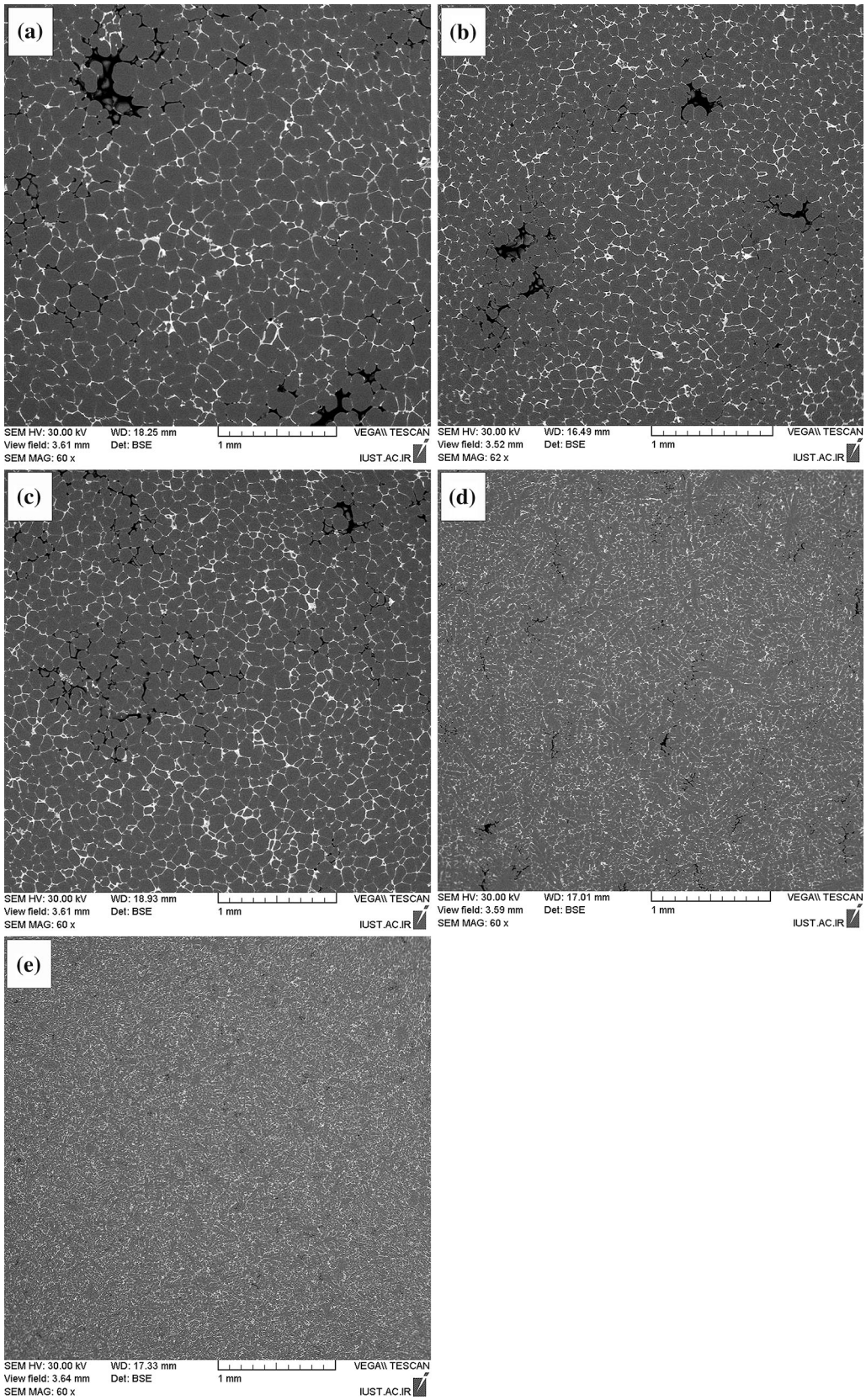

Fig. 3—Microstructural evaluation of the fraction of shrinkage porosities varied by different cooling rates; (*a*: 0.42, *b*: 0.74, *c*: 1.14, *d*: 2.46, and *e* 17.45 K s^{-1}).

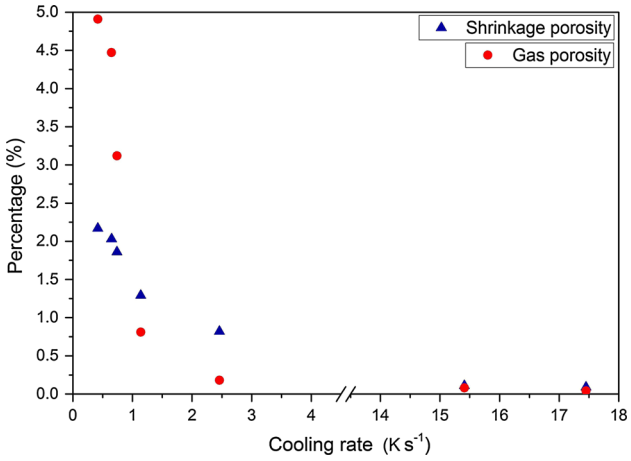

Fig. 4—The amount of cooling rates *vs* shrinkage and gas porosity formed during solidification of Al2024.

formation of shrinkage porosities during solidification is related to inadequate inter-dendritic feeding of the molten metal. According to some reports, most of solidification defects *e.g.,* shrinkage porosities, microsegregation, and hot tearing are occurred at the final stages of solidification in mushy zone.[4,18] Dendrite coherency point is referred to particular time in which mass feeding to inter-dendritic feeding is occurred due to dendrites impingement. Therefore, postponing the dendrite coherency can lead to reduce the formation of defects during solidification.[20] Also, feeding of solidified network is affected by frequency of intermetallics nucleation and the volume fraction of these phases during solidification.

According to next Section III–B, at low cooling rates, dendrite coherency has been occurred at higher temperature, compared with the higher cooling rates. There is an optimum amount of cooling rate in which the DCP has been postponed and inter-dendritic channels can be opened for a long period of time. Therefore, shrinkage porosities are reduced due to the postpone of transition between mass feeding and inter-dendritic feeding, until achieving the optimum value of cooling rate. But, at high cooling rates, kinetics of nucleation phenomenon is dominant. In spite of decreasing the solid fraction at DCP for high cooling rates condition, the frequency of nucleation is high and the amount of nuclei in a constant volume is increased. In these samples, shrinkage porosities are formed in grain boundaries and in inter-dendritic regions.[26] Since the amount of nuclei in constant volume is high, very fine shrinkage porosities distribute occasionally.

The effect of different cooling rates on gas porosities of Al2024 samples is shown in Figure 4. Samples have not been degassed in order to compare area fraction of gas porosities. The results show that area fraction of gas porosities is decreased continuously by increasing the cooling rate. Casting at a higher cooling rate leads to a corresponding refinement in pore size over the entire cross section. According to Eq. [1], in dendritic solidification, the radius of curvature of a pore is assumed to be approximately equal to the DAS/7 in casting.[22]

Table II. Effect of Cooling Rates on the Equivalent Diameter of Pores

Cooling Rate (K s^{-1})	0.42	0.65	0.74	1.14	2.46	15.41	17.45
$D_{\text{pore in Al2024}}$ (μm)	17.23	12.36	11.14	7.69	3.35	—	—

However, the size of the pores becomes very small due to very high cooling rate and thermal gradient at cooling rates used in DC casting as compared to lower cooling rates. According to Ghoncheh *et al.*[27] investigations and Eq. [1], the radius of curvature of pores in Al2024 alloy can be calculated and is listed in Table II. This equation can be used only at low cooling rates (0.42 to 2.46 K s^{-1}) and cannot predict the pore diameter at cooling rates used in DC casting process.

$$D_{\text{pore}} = 2R_{\text{pore}} = 0.2762\,(\text{DAS}) - 4.2, \qquad [1]$$

In this equation, D_{pore} is the equivalent diameter of pores.

According to correlation between DAS and cooling rate in 2024 aluminum alloy,[27] Eq. [1] can also be rewritten in the form of Eq. [2].

$$D_{\text{pores in (Al2024)}} = 0.2762\,(46.51(CR)^{-0.59}) - 4.2 \qquad [2]$$

where CR is the cooling rate.

Where the cooling rate increases, the amount of potential nucleation sites for primary α-Al phase is increased. Therefore, the fraction of nucleated primary dendrites enhances in a constant volume of the molten metal. This event causes refining of dendrites structure and decreasing the dendrite arm spacing (DAS).[27,28] In this condition, the pores are restrained by the growth of dendrite arms and formed very fine with sporadic distribution.

B. *Effect of Solidification Conditions on Dendrite Coherency Characteristics*

The formation of solidification defects is closely related to dendrite coherency temperature and solid fraction. Therefore, the effect of solidification condition was investigated on dendrite coherency parameters. According to Table III, the dendrite coherency temperature is reduced from 910.7 K to 896.9 K (637.6 °C to 623.8 °C) as the cooling rate increased. It may be caused by the kinetics of diffusion in both liquid and solid states.[29] By increasing the cooling rate, the time necessary for complete diffusion of atoms to form dendritic network becomes inadequate. Growth rate of dendrites is decreased due to the lack of diffusion process. In addition, where 0.06 wt pct Ti is added to the molten metal, the dendrite coherency temperature is reduced compared with the samples having no grain refiner. Therefore, the DCP is delayed and mass feeding to inter-dendritic feeding is postponed. So, casting defects during dendritic growth, *e.g.,* microsegregation, shrinkage, and gas porosities, are reduced. According to Johnsson[30] reports, grain size is correlated to the

Table III. Influence of Solidification Conditions on Dendrite Coherency Characteristics of Al2024

Cooling Rate (K s^{-1})	Un-Refined Samples		Grain-Refined Samples	
	T_{DCP}, K (°C)	$f_{s\ DCP}$ (Pct)	T_{DCP}, K (°C)	$f_{s\ DCP}$ (Pct)
0.42	910.7 (637.6)	10.8	908.6 (635.5)	14.1
0.65	910.3 (637.2)	14.3	907.6 (634.5)	15.8
0.74	908.5 (635.4)	14.4	907.2 (634.1)	16.1
1.14	903.0 (629.9)	28.6	904.0 (630.9)	29.1
2.46	900.1 (627.0)	21.4	903.6 (630.5)	26.4
15.41	899.5 (626.4)	7.3	900.5 (627.4)	8.6
17.45	896.9 (623.8)	7.1	895.3 (622.2)	8.3

growth rate of dendrites. As grain refiner is added, the nucleation rate is increased, but growth rate is reduced; and the dendrites can easily grow before impingement.

Solid fraction at dendrite coherency point of Al2024 alloy is given in Table III. At a constant cooling rate, the solid fraction at dendrite coherency of grain refined samples is higher than that of the samples having no grain refiner. Some investigations have been reported that dendrite coherency depends on the competition between nucleation rate and growth rate of dendrites. Since addition of Al-5Ti-1B grain refiner leads to reduce the growth rate of dendrites, inter-dendritic feeding is postponed and high percentage of solid phase can be formed before the DCP.[20]

By increasing the cooling rate, solid fraction increases initially and then decreases at higher cooling rates. Different observations are reported related to the effect of cooling rate on solid fraction at DCP. Some of them imply that as the cooling rate is increased, solid fraction at DCP is decreased; while the others have reported contradictory results.[20,26] In this research, there is an optimum amount of cooling rate, in which the maximum amount of solid fraction at DCP can be achieved. The reason is that by increasing the cooling rate, the velocity of longitudinal growth of dendrites is increased and it leads to accelerate the impingement of dendrites. The rate of lateral growth of dendrites is accelerated too. Therefore, dendrites can easily grow laterally before the coherency of dendrites starts. There is a moderate cooling rate in which a balance between the rate of longitudinal and lateral growth of dendrites is occurred. At the cooling rates higher than the optimum amount, longitudinal velocity of dendrites is dominant and at low cooling rates, lateral growth is an overcoming phenomenon.[31]

C. *Effect of Different Solidification Conditions on Microsegregation in Al2024*

Microsegregation strongly depends on different parameters, *e.g.*, alloy characteristics (chemical composition, grain refining, partition coefficient of the alloying elements), and process specific (casting speed, melt temperature, cooling rate).[18] As seen in Figure 5, by increasing the cooling rate, area fraction of eutectic phase formed in inter-dendritic regions is increased. The range of solidification temperature in Al2024 is increased by increment in cooling rates.[27] On the other words, increment of cooling rate leads to broaden the range of mushy zone. Therefore, rejection of alloying elements from dendrites to the adjacent molten metal can be occurred in a wide range of temperature and microsegregation is intensified.

Most of the alloying elements and impurities are present in aluminum alloys at hypoeutectic concentrations with $k < 1$. For example, copper and magnesium have partition coefficients of 0.17 and 0.43, respectively.[20] These alloying elements have important key roles to form the negative (solute-depleted) microsegregation in Al2024 alloy. It is also observed from Figure 5 that the area fraction of eutectic phases is increased by adding of 0.06 wt pct Ti at each constant cooling rate. Yu and Granger[32] reported negative segregation of Cu and Mg with a corresponding positive segregation of Ti in grain refined Al–Cu–Mg alloy. Also, Gariepy and Caron[33] demonstrated a direct correlation between the increasing Ti content and the magnitude of segregation.

The deleterious effect of grain refining on microsegregation is attributed to the nucleation of a larger number of free dendrites at the solidification front. Glenn *et al.*[34] invoked the formation and distribution of 'showering crystals.' They explained that small showering crystals were responsible for the negative segregation in all cases. The formation of large showering crystals, whose average solute content is higher than that of the small showering crystals, can actually lower the magnitude of negative segregation in non-grain refined samples. Low-melting second phases could weaken grain boundaries by depressing the solidus temperature of the metal and prolonging liquid film life. Also, Shabestari *et al.*[28] reported that, at each constant cooling rate, the range of solidification temperature in grain refined samples is more than that of unrefined samples. Therefore, adding of 0.06 wt pct Ti leads to broaden the range of mushy zone. Area fractions of eutectic intermetallics formed in inter-dendritic regions are summarized in Table IV.

D. *Effect of Cooling Rate and Grain Refinement on Solid Fraction Curve in Al2024*

In Figure 6, the first derivative curve of unrefined sample, the solid fraction *vs* elapsed time, and cooling curves in both unrefined and grain refined samples have been illustrated. As seen, at each constant cooling rate, the amount of solid fraction in grain refined samples is

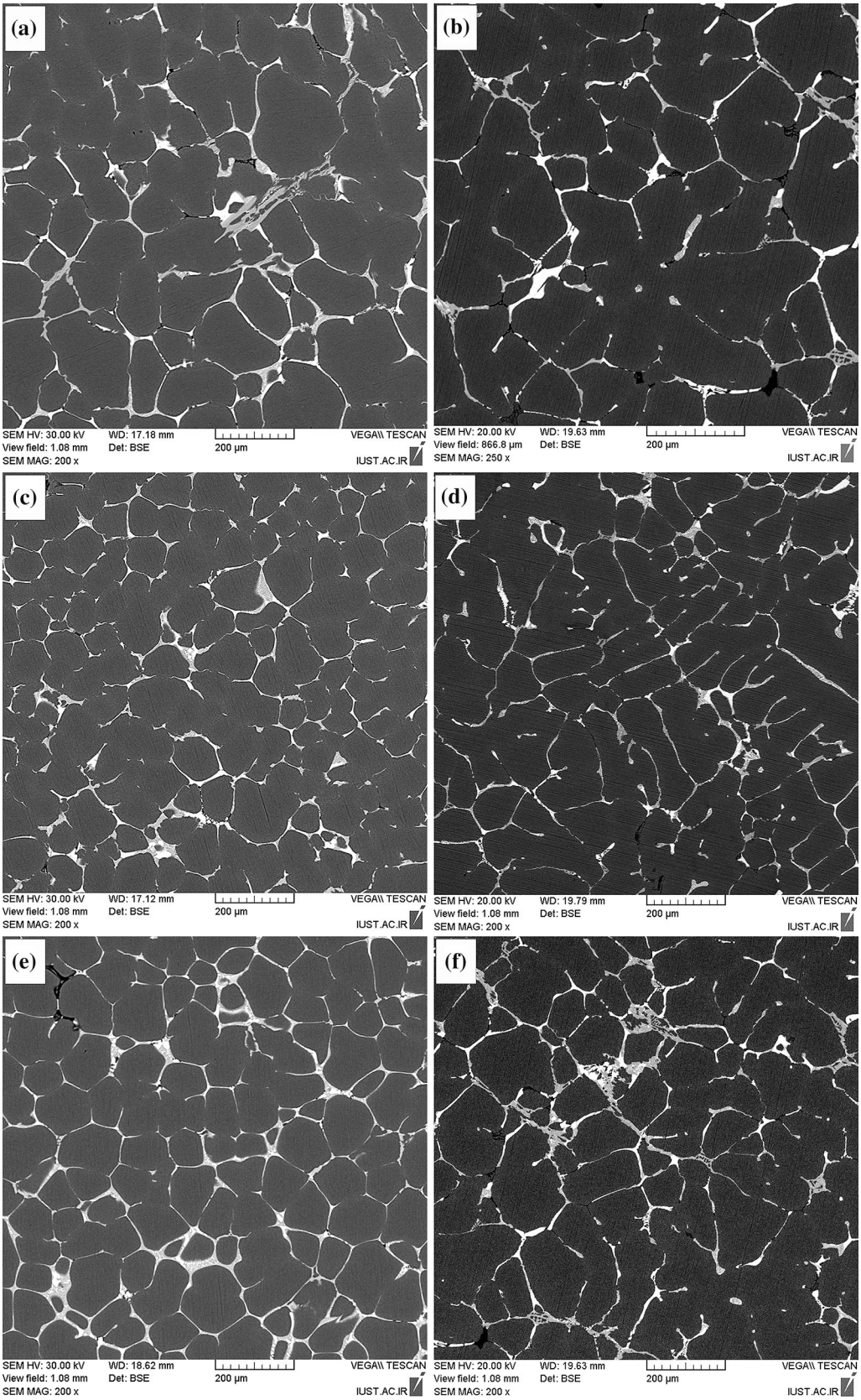

Fig. 5—Effect of different cooling rates on non-equilibrium eutectic phase in unrefined (*b*, *d*, *f*, *h*, and *j* samples) and grain refined (*a*, *c*, *e*, *g*, and *i* samples). (a and b: 0.42, c and d: 0.74, e and f: 1.14, g and h: 2.46, i and j: 17.45 K s^{-1}).

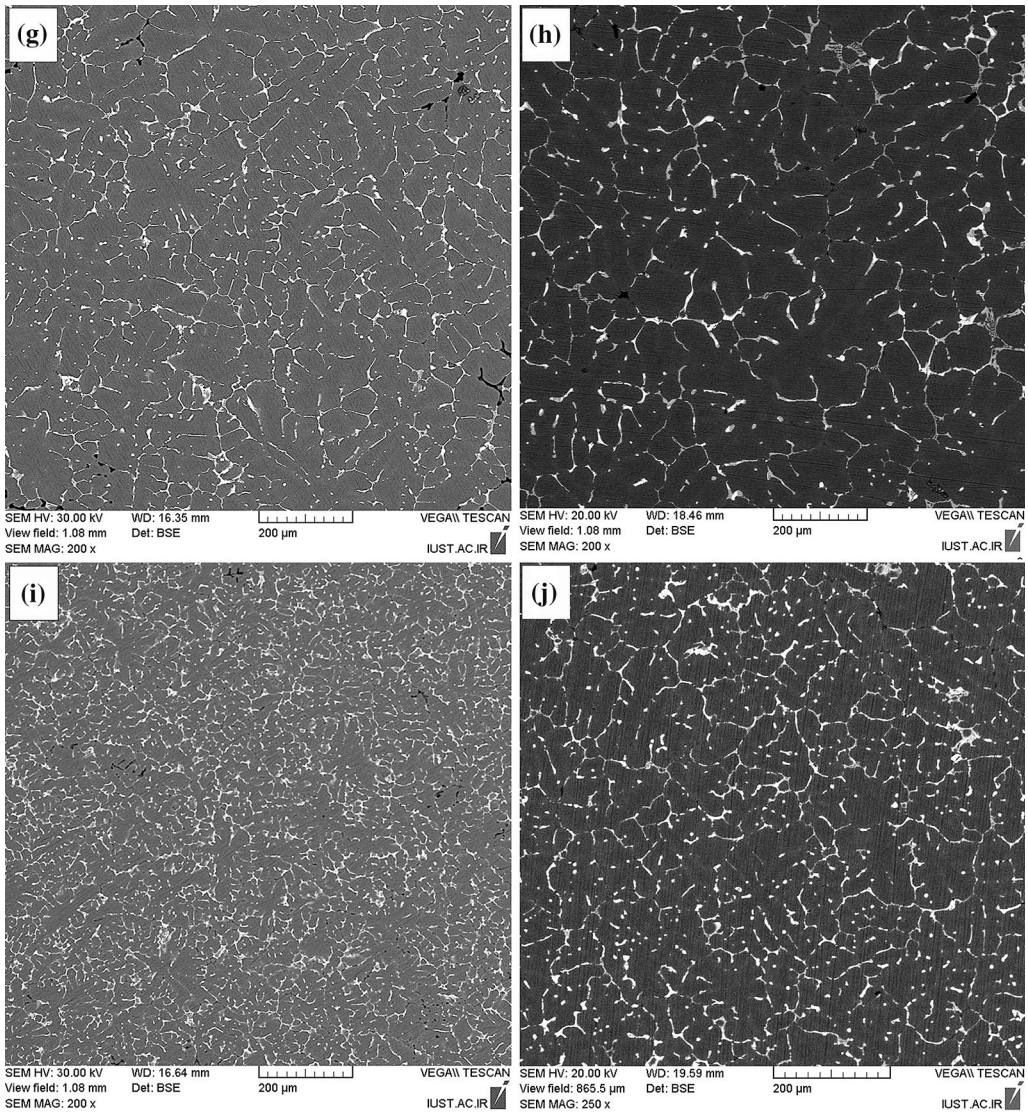

Fig. 5—continued.

higher than that of unrefined samples. In addition, by adding 0.06 wt pct Ti in the form of an Al-5Ti-1B master alloy, time interval of solidification process becomes shorter. Also, in grain refined samples, critical spent time to stabilize the initial nuclei is decreased compared with the unrefined samples. As it will be shown in section "E," solid fraction-time curves are a useful technique to calculate the hot tearing susceptibility of alloys. At low solid fraction, hot tears can be healed by a flow of liquid into the gaps in the interdendritic region since there is sufficient liquid present at this time.[31] According to the investigation reported by the authors, the hot tearing susceptibility of Al2024 alloy is occurred at later stages of solidification during the formation of Al2CuMg intermetallic compound.[28]

The presence of grain refiner leads to increase high potential substrates for nucleation, such as, $TiAl_3$, TiB_2, and $(AlTi)B_2$. Therefore, the frequency of nucleation of primary α-Al is accelerated and nucleation temperature is increased. On the other word, by adding Al-5Ti-1B grain refiner, driving force for nucleation of stable nuclei in a molten metal is increased and nucleation is occurred easier. Increasing the potential nucleation sites at grain refined samples leads to accelerating the solidification process.[20,27] In this condition, solidification is finished more rapidly, and the amount of solid fraction at each time is more than that of the samples having no grain refiner.

E. *Hot Tearing Susceptibility of Al2024 Using Clyne and Davies' Criterion*

According to Clyne and Davies' criterion,[11,13] hot tearing susceptibility is calculated by Eq. [3]:

$$\mathrm{HCSC} = \frac{t_V}{t_R} = \frac{t_{0.99} - t_{0.9}}{t_{0.9} - t_{0.4}}. \quad [3]$$

The hot cracking sensitivity coefficient (HCSC) is defined by the ratio of the vulnerable time period, where

hot tearing may develop (t_v), and time available for the stress-relief process, where mass feeding and liquid feeding occur (t_R).

In this equation, $t_{0.99}$ is the time when the volume fraction of solid, f_s, is 0.99, $t_{0.9}$ is the time when f_s is 0.9, and $t_{0.4}$ is the time when f_s is 0.4.

Using Clyne and Davies' criterion, hot tearing susceptibility of Al2024 has been shown in Figures 6 and 7. According to Figure 7, by increasing the cooling rate, hot tearing susceptibility reduces initially and then increases at higher cooling rates. Feeding mode of solidified network is strongly affected by nucleation of eutectic phase.[35] This parameter has a key role on the hot tearing susceptibility. At low cooling rates, the dendrite coherency is occurred faster than the medium cooling rate condition.[20] Thus, mass feeding to inter-dendritic feeding is accelerated and dendrite coherency hinders perfect feeding of solidified network. At medium cooling rate condition, solid fraction at each time is more than the samples solidified at low cooling rates; and inter-dendritic channels will be opened for a longer time. Increasing hot tearing susceptibility at higher cooling rates can be caused by the following:

Table IV. Effect of Solidification Conditions on Fraction of Non-Equilibrium Eutectic Phases

Cooling Rate (K s^{-1})	Non-Equilibrium Eutectic Fraction (Pct)	
	Un-Refined Samples	Grain-Refined Samples
0.42	7.7	9.1
0.65	8.0	10.2
0.74	8.2	10.7
1.14	8.6	11.2
2.46	7.2	11.7
15.41	8.8	13.9
17.45	9.1	14.5

(1) The twofold effect of increasing the cooling rate on hot tearing can be divided to two regions: (a) low to medium cooling rates, (b) high cooling rates.

According to Table IV and Figure 5, by increasing the cooling rates, volume fraction of eutectic phase at inter-dendritic regions and grain boundaries has been increased. Since stress accommodations and healing phenomena are more significant with increasing amount of eutectic, hot tearing tendency decreases with increasing the volume fraction of eutectic.[6] This condition is overcoming phenomenon at low to medium cooling rate interval (0.42 to 2.46 K s^{-1}).

But at high cooling rates such as cooling rates used in DC casting process, reducing in solid fraction is occurred due to acceleration of longitudinal growth of dendrites. In this condition, the dendrite coherency point is occurred rapidly and complete mass feeding becomes more difficult.[20,36] In addition, By increasing the cooling rate, the temperature range of the mushy zone becomes broaden and the structure is more exposed to temperature interval of hot cracking susceptible. A large freezing range of an alloy promotes hot tearing because such an alloy spends a longer time in the vulnerable state in which thin liquid films exist between the dendrites. The liquid film surrounding the grain at later stages of solidification is considered as a stress concentrator of the semi-solids body.[12] Tensile stress caused by contraction is highly concentrated in these liquid. In this theory, a liquid cavity acts as a crack initiator.[6,12] Generally, alloys with broad freezing range are exposed to hot cracking defects.[37]

(2) According to research done by Li *et al.*,[38] solidification of molten metal in the molds, which have not

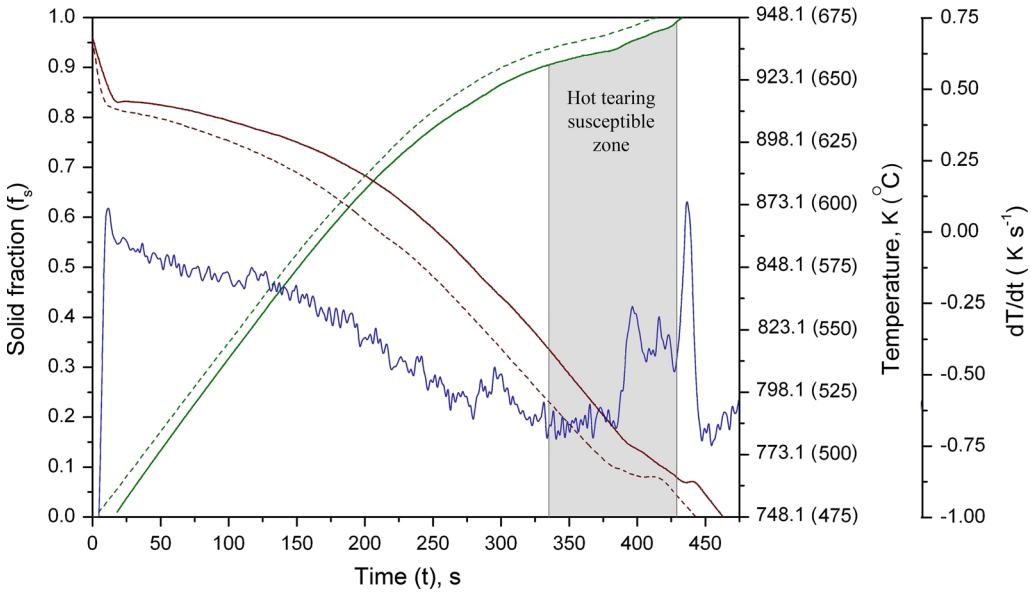

Fig. 6—Cooling curves, solid fraction *vs* time, and first derivative curve of Al2024 at cooling rate of 0.65 K s^{-1} (straight line: unrefined, and dash-marked line: grain refined sample).

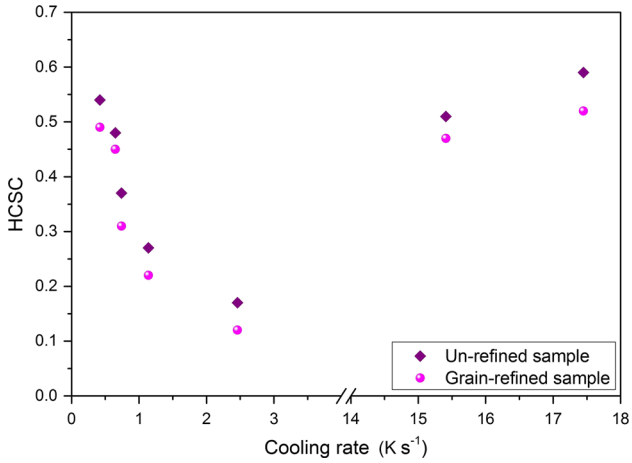

Fig. 7—Effect of cooling rate and grain refiner on hot cracking susceptibility criterion (HCSC) of Al2024.

been preheated or preheated at low temperature, is accompanied by the enhancement of hot tearing susceptibility. This was probably because that higher mold temperature improved feeding. Also, at higher mold temperature, the cracks could be refilled by the remaining liquid and healed.[6]

(3) Lin[39] showed that another significant parameter on hot cracking is the presence of gas bubbles in the molten metal. Accordingly, samples with high amount of entrained gas bubbles are less susceptible to hot cracking defects. The presence of gas in the molten metal leads to applying locally pressure to the melt. This pressure facilitates the inter-dendritic diffusion. Also, gas bubbles increase the resistance of solidifying structure against shrinkage porosities generated during solidification. According to section "A" of results and discussion, by increasing the cooling rate, gas porosities which exist in samples are reduced. Conversely, shrinkage porosities have deleterious effects on hot cracking susceptibility. The detrimental role of shrinkage porosities can be considered from two aspects:

  (a) According to the two-phase model of the semi-solid dendritic network, the pressure depression of liquid phase occurred in the mushy zone leads to generate a chain of pores or cavities. The crack may nucleate or develop from any structural defects can be propagate through these pores.[38]
  (b) Shrinkage porosities usually act as a stress concentrator. Local critical stress leads to initiation and propagation of cracks during solidification.[39]

(4) By adding grain refiner, the hot tearing susceptibility is decreased at each constant cooling rate. This may caused by some reasons written below:

  (a) The main reason is related to the dendrite coherency. As 0.06 wt pct Ti in the form of an Al-5-Ti-1B grain refiner is added to the molten metal, the dendrite coherency temperature is reduced compared with the samples having no grain refiner.[40] Therefore, the DCP is postponed and mass feeding to inter-dendritic feeding is delayed. In this condition, casting defects during equiaxed dendritic growth, *e.g.,* microsegregation, shrinkage, porosity, and hot tearing, are reduced.
  (b) It was explained that the size of grain was important as it affected the mode of eutectic distribution. When the eutectic was present at the grain boundaries, it had the maximum effect on permitting free movement of the grains to accommodate the contraction of the casting.[38] Consequently, hot tearing tendency was reduced. Finer primary grains lead to increasing the probability of eutectic being present at grain boundaries.[38]
  (c) With the addition of grain refinement, the mush becomes more pliable, *i.e.*, more liquid-like, and the point, at which the mush began to behave more like a solid than a liquid, was delayed, which reduces the severity of hot tearing.[41] It was concluded that grain refinement decreased the hot tearing susceptibility through changing the grain morphology from columnar to equiaxed and reducing the grain size.
  (d) Changing the liquid film thickness between grains leads to changing the capillary pressures.[42] Smaller grain size implies thinner liquid films between grains and therefore greater capillary pressures to be overcome before a tear propagates. Easton *et al.* showed that the load development vs. temperature was slowed down and load was lowered with addition of grain refiner.[42]

F. *Effect of Solidification Conditions on Hardness of Samples*

As seen in Figure 8, the value of hardness of the specimens is increased by cooling rate. According to the other investigation carried out by the authors, increasing the cooling rate from 0.4 to 17.5 K s^{-1} leads to reduce dendrite arm spacing about 89 pct.[27] Also, as the cooling rate increases, the content of both gas and shrinkage porosities are decreased and distribution of these defects becomes more uniform. In addition, hard intermetallic compounds in Al2024 alloy, *e.g.,* Al_2CuMg, Mg_2Si, $Al_{15}(CuFeMn)_3Si_2$ phases are refined and distributed uniformly.[28] Therefore, they lead to increase the hardness value by the enhancement of the cooling rates.

According to Figure 8, at each constant cooling rate, grain refining of the structure increases the hardness of the samples. The presence of more suitable substrates for nucleation and the higher amount of solid fraction in the grain refined samples cause the increased hardness.

IV. CONCLUSIONS

The effect of cooling rate and adding 0.6 wt pct Ti grain refiner on the formation of some defects during solidification of Al2024 alloy such as, hot tearing, microsegregation, and gas and shrinkage porosities were studied. The results are summarized as follows:

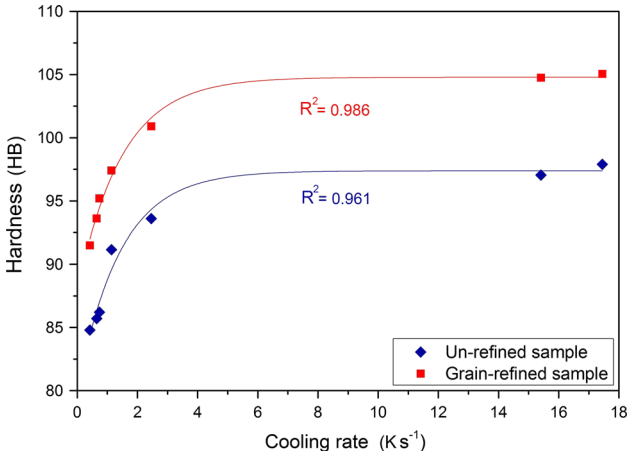

Fig. 8—Influence of cooling rate and grain refiner on the hardness of Al2024 samples.

(1) By increasing the cooling rate, the area fraction of both gas and shrinkage porosities reduces considerably in Al2024 alloy. At two cooling rates of 15.41 and 17.45 K s^{-1}, the amount of shrinkage porosity is close to zero.
(2) As the cooling rate increases, the dendrite coherency temperature is reduced from 910.7 K to 896.9 K (637.6 °C to 623.8 °C) and solid fraction at dendrite coherency point increases initially and then decreases at higher cooling rates.
(3) The increment of cooling rate leads to increasing the area fraction of eutectic phase formed in inter-dendritic regions. Also, the amount of microsegregation is increased by adding of 0.06 wt pct Ti at each constant cooling rate.
(4) By increasing the cooling rate, hot tearing susceptibility reduces initially and then increases at higher cooling rates. The hot tearing susceptibility is decreased at each constant cooling rate by adding grain refiner.

ACKNOWLEDGEMENT

The authors would like to acknowledge the Center of Excellence for High Strength Alloys Technology (CEHSAT) of Iran University of Science and Technology (IUST).

REFERENCES

1. D.G. Eskin: *Physical Metallurgy of Direct-Chill Casting Aluminum Alloys*, Taylor and Francis group, New York, 2008.
2. M.H. Nasresfahani and M.J. Rajabloo: *Metall. Mater. Trans. B*, 2014, vol. 45B, pp. 1827–33.
3. P. Kotas, C.C. Tutum, J. Thorborg, and J. Henri Hattel: *Metall. Mater. Trans. B*, 2012, vol. 43B, pp. 609–26.
4. D.G. Eskin, Suyitno, and L. Katgerman: *Prog. Mater. Sci.*, 2004, vol. 49, pp. 629–11.
5. S. Lin, C. Aliravci, and M.O. Pekguleryuz: *Metall. Mater. Trans. A*, 2007, vol. 38A, pp. 1056–68.
6. M. Easton, J.F. Grandfield, D.H. StJohn, and B. Rinderer: *Mater. Sci. Forum.*, 2006, vol. 519, pp. 1675–80.
7. M. Easton, D.H. StJohn, and L. Sweet: *Mater. Sci. Forum.*, 2009, vol. 630, pp. 213–21.
8. Sh. Li, K. Sadayappan, and D. Apelian: *Metall. Mater. Trans. B*, 2013, vol. 44B, pp. 614–23.
9. Suyitno, D.G. Eskin, and L. Katgerman: *Mater. Sci. Eng. A*, 2006, vol. 420, pp. 1–7.
10. U. Feurer: *Delft University of Technology*, The Netherlands, 1977, pp. 131–45.
11. T.W. Clyne, and G.J. Davies: *Metals Society, London,* 1979, pp. 274–78.
12. Suyitno, W.H. Kool, and L. Katgerman: *Metall. Mater. Trans. A*, 2005, vol. 36A, pp. 1537–46.
13. T.W. Clyne and G.J. Davies: *Br. Foundryman*, 1975, vol. 68, pp. 238–44.
14. I.I. Novikov: *Goryachetomkost Tsvetnykh Metallov i Splavov*, Nauka, Moscow, 1966.
15. N.N. Prokhorov: *Russian Cast. Prod.*, 1962, vol. 2, pp. 172–75.
16. Ch. Monroe and Ch. Beckerman: *JOM*, 2014, vol. 66, pp. 1439–45.
17. M. Rappaz, J.M. Drezet, and M. Gremaud: *Metall. Mater. Trans. A*, 1999, vol. 30A, pp. 449–55.
18. R. Nadella, D.G. Eskin, Q. Du, and L. Katgerman: *Prog. Mater. Sci.*, 2008, vol. 53, pp. 421–80.
19. M.R. Ridolfi: *Metall. Mater. Trans. B*, 2014, vol. 45B, pp. 1425–38.
20. M. Malekan and S.G. Shabestari: *Metall. Mater. Trans. A*, 2009, vol. 40A, pp. 3196–03.
21. P.D. Lee, R.C. Atwood, R.J. Dashwood, and H. Nagaumi: *Mater. Sci. Eng. A*, 2002, vol. 328, pp. 213–22.
22. D.J. Lahaie and M. Bouchard: *Metall. Mater. Trans. B*, 2001, vol. 32B, pp. 697–705.
23. X. Yan and J.C. Lin: *Metall. Mater. Trans. B*, 2006, vol. 37, pp. 913–18.
24. R.G. Santos and M.L.N.M. Melo: *Mater. Sci. Eng. A*, 2005, vol. 391, pp. 151–58.
25. N. Roy, A.M. Samuel, and F.H. Samuel: *Metall. Mater. Trans. A*, 1996, vol. 27A, pp. 415–29.
26. R. Chavez-Zamarripa, J.A. Ramos-Salas, J. Talamantes-Silva, S. Valtierra, and R. Colas: *Metall. Mater. Trans. A*, 2007, vol. 38A, pp. 1875–79.
27. M.H. Ghoncheh, S.G. Shabestari, and M.H. Abbasi: *J. Therm. Anal. Calorim.*, 2014, vol. 117, pp. 1253–61.
28. S.G. Shabestari, M.H. Ghoncheh, and H. Momeni: *Thermochim. Acta.*, 2014, vol. 589, pp. 174–82.
29. H. Mehrer: *Diffusion in solids*, 1st ed., Springer, Berlin, 2007.
30. M. Johnsson, L. Backerud, and G.K. Sigworth: *Metall. Mater. Trans. A*, 1993, vol. 24A, pp. 481–91.
31. M.H. Ghoncheh and S.G. Shabestari: *Metall. Mater. Trans. A*, 2015, vol. 46A, pp. 1287–99.
32. F.Y. Xie, T. Kraft, Y. Zuo, C.H. Moon, and Y.A. Chang: *Acta Mater.*, 1999, vol. 47, pp. 489–500.
33. X. Yan, S. Chen, F. Xie, and Y.A. Chang: *Acta Mater.*, 2002, vol. 50, pp. 2199–07.
34. P.D. Lee, A. Chirazi, R.C. Atwood, and W. Wang: *Mater. Sci. Eng. A*, 2004, vol. 365, pp. 57–65.
35. S.G. Shabestari and S. Ghodrat: *Mater. Sci. Eng. A*, 2007, vol. 467, pp. 150–58.
36. Y.F. Guven and J.D. Hunt: *Cast. Metals.*, 1988, vol. 1, pp. 104–11.
37. H. Chadwick: *Cast. Metals.*, 1991, vol. 4, pp. 43–49.
38. S. Li: Ph.D. thesis, Worcester Polytechnic Institute, 2010.
39. S. Lin: Ph.D. thesis, Université du Québec à Chicoutimi, 1999.
40. N. Jamaly, A.B. Phillion, and J.M. Drezet: *Metall. Mater. Trans. B*, 2013, vol. 44B, pp. 1287–95.
41. M.B. Djurdjevic and G. Huber: *J. Alloy. Compd.*, 2014, vol. 590, pp. 500–06.
42. M. Easton, H. Wang, J. Grandfield, D.H. StJohn, and E. Sweet: *Mater. Forum.*, 2004, vol. 28, pp. 224–29.